Appl. Math. Mech. -Engl. Ed., **40**(8), 1211–1226 (2019)

Applied Mathematics and Mechanics (English Edition)

https://doi.org/10.1007/s10483-019-2508-6

Wavelet analysis of stagnation point flow of non-Newtonian nanofluid*

M. HAMID[1], M. USMAN[2,3], R. U. HAQ[4], Z. H. KHAN[5,6,†], Wei WANG[1]

1. School of Mathematical Sciences, Peking University, Beijing 100871, China;
2. BIC-ESAT, College of Engineering, Peking University, Beijing 100871, China;
3. State Key Laboratory for Turbulence and Complex Systems, Department of Mechanics and Engineering Science, Peking University, Beijing 100871, China;
4. Department of Electrical Engineering, Bahria University, Islamabad 44000, Pakistan;
5. State Key Laboratory of Hydraulics and Mountain River Engineering, College of Water Resource & Hydropower, Sichuan University, Chengdu 610065, China;
6. Key Laboratory of Advanced Reactor Engineering and Safety, Ministry of Education, Tsinghua University, Beijing 100084, China

(Received Dec. 7, 2018 / Revised Jan. 28, 2019)

Abstract The wavelet approach is introduced to study the influence of the natural convection stagnation point flow of the Williamson fluid in the presence of thermophysical and Brownian motion effects. The thermal radiation effects are considered along a permeable stretching surface. The nonlinear problem is simulated numerically by using a novel algorithm based upon the Chebyshev wavelets. It is noticed that the velocity of the Williamson fluid increases for assisting flow cases while decreases for opposing flow cases when the unsteadiness and suction parameters increase, and the magnetic effect on the velocity increases for opposing flow cases while decreases for assisting flow cases. When the thermal radiation parameter, the Dufour number, and Williamson's fluid parameter increase, the temperature increases for both assisting and opposing flow cases. Meanwhile, the temperature decreases when the Prandtl number increases. The concentration decreases when the Soret parameter increases, while increases when the Schmidt number increases. It is perceived that the assisting force decreases more than the opposing force. The findings endorse the credibility of the proposed algorithm, and could be extended to other nonlinear problems with complex nature.

Key words Williamson nanofluid, heat and mass transfer, stagnation point flow, assisting and opposing flow, Chebyshev wavelet method

Chinese Library Classification O361
2010 Mathematics Subject Classification 42C40, 76A05, 76W05

∗ Citation: HAMID, M., USMAN, M., HAQ, R. U., KHAN, Z. H., and WANG, W. Wavelet analysis of stagnation point flow of non-Newtonian nanofluid. *Applied Mathematics and Mechanics* (*English Edition*), **40**(8), 1211–1226 (2019) https://doi.org/10.1007/s10483-019-2508-6

† Corresponding author, E-mail: zafarhayyatkhan@gmail.com

Project supported by the National Natural Science Foundation of China (Nos. 51709191, 51706149, and 51606130), the Key Laboratory of Advanced Reactor Engineering and Safety, Ministry of Education of China (No. ARES-2018-10), and the State Key Laboratory of Hydraulics and Mountain River Engineering of Sichuan University of China (No. Skhl1803)

©Shanghai University and Springer-Verlag GmbH Germany, part of Springer Nature 2019

Nomenclature

λ,	Buoyancy effect due to the temperature difference;	A,	unsteadiness parameter;
λ^*,	Buoyancy effect due to the concentration difference;	σ^*,	Boltzmann constant;
k^*,	coefficient of the mean absorption;	k^{T},	concentration susceptibility;
β_{C},	coefficient of the concentration expansion;	Γ,	coefficient of the Williamson fluid;
ρ,	density of the fluid;	β_{T},	coefficient of thermal expansion;
σ,	electrical conductivity;	Du,	Dufour number;
M,	Hartmann number;	g,	gravitational acceleration;
B,	magnetic field strength;	ν,	kinematic viscosity;
T_{m},	mean fluid temperature;	D_{B},	mass diffusivity coefficient;
c_s,	ratio of the thermal diffusion;	Pr,	Prandtl number;
Re,	Reynolds number;	R,	ratio of λ^* to λ;
r,	stagnation point parameter;	c_p,	specific heat;
Sr,	Soret number;	S,	suction parameter;
k,	thermal conductivity;	Sc,	Schmidt number;
		Rd,	thermal radiation;
		Λ,	Williamson fluid parameter.

1 Introduction

The empathetic nature of non-Newtonian flows and motion near a stagnation region of a solid body needs more investigations recently due to its vital applications in industry, engineering, and other sciences. The thermal oil recovery, high-speed flows, and thrust bearing are few scientific applications, where the role of the Said mechanism is very frequent. The stagnation area of the solid body could be a moving surface or a fixed area in the liquid. The pioneering effort in this domain is presented by Hiemenz[1], where the two-dimensional (2D) Navier-Stokes equations were transformed into the nonlinear ordinary differential form, and the exact solutions were obtained. Later on, Homann and Angew[2] reported the three-dimensional axisymmetric stagnation point flow, and obtained the similarity solution of the modeled problem. After these pioneering investigations, several researchers carried out this specific domain by means of different aspects and mechanisms. Makinde et al.[3] analyzed the influence of buoyancy on the heat transfer and magnetohydrodynamics (MHD) stagnation point nanofluid flow past a convectively heated stretching/shrinking sheet. They showed that, an increase in the buoyancy force intensity resulted in an increase in the local Nusselt number while a decrease in the skin friction coefficient and the local Sherwood number. Haq et al.[4] studied the influence of thermal radiation and slip on the MHD stagnation point nanofluid flow over a stretching sheet. They showed that, the velocity profile was enhanced when the ratio of the free stream velocity increased, and the temperature profile dropped when the thermal slip parameter increased. Hayat et al.[5] numerically examined the radiation and melting heat transfer impacts on the stagnation point flow of the carbon-H_2O nanofluid. Tarakaramu and Narayana[6] examined the Joule heating and nonlinear thermal radiation effects on the MHD stagnation point flow of a nanofluid over a convectively heated stretching surface. They showed that, when the temperature ratio parameter increased, the rate of heat transfer increased. For more details about such research, one may refer to Refs. [7]−[11] and the references therein.

Recently, nanotechnology and heat transport come to be hot topics of research due to their vigorous roles in scientific and practical applications, e.g., solar water heating, engine cooling, and drilling[12]. Choi[13] made a pioneering contribution to improve the heat transfer rate. Buongiorno[14] and Tiwari and Das[15] proposed mathematical models to study nanofluids. Hayat et al.[16] studied the Joule heating and slip impacts in mixed convection peristaltic transport of nanofluids. Reddy and Chamkha[17] analyzed the MHD convective flow of TiO_2-water and Al_2O_3-water nanofluids past a stretching sheet in porous media. For more details

about nanofluids, one may refer to Refs. [18]−[21].

The nature of non-Newtonian fluids is complex as compared with that of Newtonian fluids, and many models have been proposed. Williamsonin presented a non-Newtonian nanofluid model in 1929, where the flow of pseudoplastic materials was analyzed experimentally[22]. The flow model has been successfully used in fields such as the preparation of emulsions and the extrusion of polymer sheets. Amanulla et al.[23] numerically explored the effects of the Biot number and the thermal radiation on the MHD Williamson fluid flow over a vertical convective surface. Jain and Parmar[24] carried out a detailed study on the radiation effects on the MHD Williamson fluid flow over a stretching cylinder through a porous medium with heat source. Recently, Hamid et al.[25] performed a numerical study on the unsteady MHD Williamson nanofluid flow in a permeable channel, and analyzed the effects of thermal radiation and the heat source/sink. Mustafa et al.[26] examined the effects of buoyancy on the MHD nanofluid flow past a vertical surface with the activation energy and chemical reaction. They showed that the thermal boundary layer thickness decreased due to the concentration and temperature differences as well as the buoyancy, and the mixed convection parameter was directly proportional to the velocity of the fluid. For more details about natural convection, one may refer to Refs. [7] and [27]−[29].

The motivation of the current work is to analyze the effects of buoyancy assisting and opposing on the stagnation point flow of the Williamson nanofluid in the presence of thermal radiation. Appropriate similarity techniques transform the governing flow equations into a nonlinear system of ordinary differential equations. Numerical simulations are performed by means of the Chebyshev wavelet method. The significant effects of the emerging parameters are presented graphically. It is concluded that the modification in traditional Chebyshev wavelets brings more accuracy and it is a compatible technique to tackle nonlinear flow problems.

2 Mathematical and geometrical analysis

Consider the 2D unsteady viscous stagnation point flow of an incompressible Williamson nanofluid past a permeable stretched surface (see Fig. 1). The velocity is

$$u_{\mathrm{w}} = cx/(1-\epsilon t),$$

where c and ϵ are the stretching coefficient and the unsteadiness of the problem, respectively,

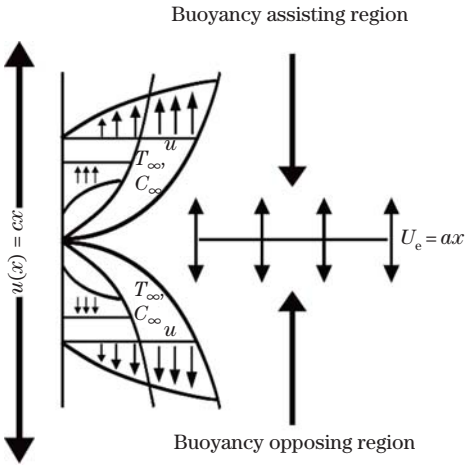

Fig. 1 Geometry of the problem

and $\epsilon > 0$. The free stream velocity is

$$u_{\mathrm{e}} = ax/(1-\epsilon t),$$

where $a > 0$ is the stagnation flow strength. Further, we assume that the temperature and the concentration at the sheet are, respectively, as follows:

$$T_{\mathrm{w}} = T_\infty + \frac{b}{1-\epsilon t}x, \quad C_{\mathrm{w}} = C_\infty + \frac{b}{1-\epsilon t}x,$$

where $b > 0$. The ambient temperature and concentration are defined as T_∞ and C_∞, respectively. Moreover, in the y-axis direction (normal to the sheet), a magnetic field having the strength B is applied. The effects of the Soret and Dufour numbers are considered. The above restrictions provide a modeled mathematical problem as follows:

$$\frac{\partial u}{\partial x} + \frac{\partial v}{\partial y} = 0, \tag{1}$$

$$\begin{aligned}&\frac{\partial u}{\partial t} + u\frac{\partial u}{\partial x} + v\frac{\partial u}{\partial y}\\ &= \frac{\partial u_{\mathrm{e}}}{\partial t} + u_{\mathrm{e}}\frac{\partial u_{\mathrm{e}}}{\partial x} + \nu\frac{\partial^2 u}{\partial y^2} + \sqrt{2}\nu\Gamma\Big(\frac{\partial u}{\partial y}\Big)\Big(\frac{\partial^2 u}{\partial y^2}\Big)\\ &\pm g(\beta_{\mathrm{T}}(T-T_\infty) + \beta_{\mathrm{C}}(C-C_\infty)) - \frac{\sigma B}{\rho}(u-u_{\mathrm{e}}),\end{aligned} \tag{2}$$

$$\frac{\partial T}{\partial t} + u\frac{\partial T}{\partial x} + v\frac{\partial T}{\partial y} = \frac{k}{\rho c_p}\frac{\partial^2 T}{\partial y^2} + \frac{16\sigma^* T_\infty^3}{3k^*\rho c_p}\frac{\partial^2 T}{\partial y^2} + \frac{D_{\mathrm{B}}k_{\mathrm{T}}}{c_s c_p}\frac{\partial^2 C}{\partial y^2}, \tag{3}$$

$$\frac{\partial C}{\partial t} + u\frac{\partial C}{\partial x} + v\frac{\partial C}{\partial y} = D_{\mathrm{B}}\frac{\partial^2 T}{\partial y^2} + \frac{D_{\mathrm{B}}k_{\mathrm{T}}}{T_{\mathrm{m}}}\frac{\partial^2 T}{\partial y^2}, \tag{4}$$

$$\begin{cases} u = u_{\mathrm{w}}, \quad v = -\dfrac{v_0}{\sqrt{1-\epsilon t}}, \quad T = T_{\mathrm{w}}, \quad C = C_{\mathrm{w}} \quad \text{at} \quad y = 0,\\ u = u_{\mathrm{e}}, \quad C = C_\infty, \quad T = T_\infty \quad \text{as} \quad y \to \infty, \end{cases} \tag{5}$$

where u and v are the velocity components along the x- and y-axes, respectively. σ is the electrical conductivity. ν is the kinematic viscosity. Γ is the coefficient of the Williamson fluid. β_{T} is the coefficient of thermal expansion. g is the gravitational acceleration. β_{C} is the coefficient of concentration expansion. B is the magnetic field strength. ρ is the density. k is the thermal conductivity. c_s is the ratio of thermal diffusion. σ^* is the Boltzmann constant. c_p is the specific heat. k^* is the coefficient of mean absorption. D_{B} is the mass diffusivity coefficient. k_{T} is the concentration susceptibility. T_{m} is the mean fluid temperature.

The following similarity transformations are used to nondimensionalize the nonlinear flow equations (1)−(5)[10]:

$$\begin{cases} u = \dfrac{cx}{1-\epsilon t}F'(\eta), \quad v = -\sqrt{\dfrac{c\nu}{1-\epsilon t}}F(\eta), \quad \theta = \dfrac{T-T_\infty}{T_{\mathrm{w}}-T_\infty},\\ \phi = \dfrac{C-C_\infty}{C_{\mathrm{w}}-C_\infty}, \quad \eta = \sqrt{\dfrac{c}{(1-\epsilon t)\nu}}y. \end{cases} \tag{6}$$

The partial differential equation (PDE) system (2)−(5) takes the following form after incorporating the similarity variables in Eq. (6):

$$(1+\Lambda F''(\eta))F'''(\eta) - F'^2(\eta) + (F(\eta) - A\eta/2)F''(\eta) - M(r+F'(\eta)) + A(r-F'(\eta)) \pm \lambda(\theta(\eta) + R\phi(\eta)) + r^2 = 0, \tag{7}$$

$$(1+Rd)\theta''(\eta) + Pr(F(\eta) - A\eta/2)\theta'(\eta) + PrDu\phi''(\eta) = 0, \tag{8}$$

$$\phi''(\eta) + Sc(F(\eta) - A\eta/2)\phi'(\eta) + SrSc\theta''(\eta) = 0. \tag{9}$$

The boundary conditions are

$$\begin{cases} F(\eta) = S, \quad F'(\eta) = 1, \quad \theta(\eta) = \phi(\eta) = 1 \quad \text{for} \quad \eta = 0, \\ F'(\eta) = r, \quad \theta(\eta) = \phi(\eta) = 0 \quad \text{as} \quad \eta \to \infty. \end{cases} \tag{10}$$

In Eqs. (7)–(10), $\pm$ characterize the assisting flow and the opposing flow, respectively, and $R > 0$. Λ is the Williamson fluid parameter. A is the unsteadiness parameter. M is the Hartmann number. λ represents the buoyancy effect due to the temperature difference. λ^* represents the buoyancy effect due to the concentration difference. R is the ratio of λ^* to λ. r is the stagnation point parameter. Rd is the thermal radiation. Du is the Dufour number. Pr is the Prandtl number. Sr is the Soret number. $S > 0$ is the suction parameter. They are defined as follows:

$$\begin{cases} \Lambda = \dfrac{\sqrt{2}\Gamma x c^{3/2}}{\sqrt{\nu}}, \quad A = \dfrac{\epsilon}{c}, \quad M = \dfrac{B^2\sigma}{\rho c}, \\ \lambda = \dfrac{Gr_{\mathrm{T}}}{Re_x^2}, \quad Gr_{\mathrm{T}} = \dfrac{\beta g(T_{\mathrm{w}} - T_\infty)}{\nu^2}, \quad Re_x = \dfrac{xu_{\mathrm{e}}}{\nu}, \\ R = \dfrac{\lambda^*}{\lambda}, \quad \lambda^* = \dfrac{Gr_{\mathrm{C}}}{Re_x}, \quad Gr_{\mathrm{C}} = \dfrac{\beta g(T_{\mathrm{w}} - T_\infty)}{\nu^2}, \\ r = \dfrac{a}{c}, \quad Rd = \dfrac{16\sigma^* T_\infty^3}{3kk^*}, \quad Pr = \dfrac{\nu}{\alpha}, \quad Sc = \dfrac{\nu}{D_{\mathrm{B}}}, \\ Du = \dfrac{(C_{\mathrm{w}} - C_\infty)D_{\mathrm{B}}k_{\mathrm{T}}}{\nu(T_{\mathrm{w}} - T_\infty)c_p c_s}, \quad Sr = \dfrac{(T_{\mathrm{w}} - T_\infty)k_{\mathrm{T}}D_{\mathrm{B}}}{\nu(C_{\mathrm{w}} - C_\infty)T_{\mathrm{m}}}, \quad S = \dfrac{v_0}{\sqrt{\nu c}}. \end{cases}$$

The skin friction coefficient (C_{f}), the local Nusselt number (Nu), and the Sherwood number (Sh) are the physical quantities of interest, and are given as follows:

$$\begin{cases} C_{\mathrm{f}} = \dfrac{\mu}{\rho u_{\mathrm{w}}^2}\Big(\dfrac{\partial u}{\partial y} + \dfrac{\Gamma}{\sqrt{2}}\Big(\dfrac{\partial u}{\partial y}\Big)^2\Big)_{y=0}, \\ Nu = -\dfrac{kx}{k(T_{\mathrm{w}} - T_\infty)}\Big(\dfrac{\partial T}{\partial y}\Big)_{y=0}, \\ Sh = -\dfrac{D_{\mathrm{B}}x}{D_{\mathrm{B}}(C_{\mathrm{w}} - C_\infty)}\Big(\dfrac{\partial C}{\partial y}\Big)_{y=0}. \end{cases}$$

By means of Eq. (6), the nondimensional form of the skin friction coefficient C_{f}, the local Nusselt number Nu, and the Sherwood number Sh are

$$\begin{cases} \sqrt{Re}C_{\mathrm{f}} = \Big(F''(0) + \dfrac{\Lambda}{2}F''^2(0)\Big), \\ \dfrac{Nu}{\sqrt{Re}} = -(1+Rd)\theta'(0), \\ \dfrac{Sh}{\sqrt{Re}} = -\phi'(0), \end{cases} \tag{11}$$

where $Re = xu_{\mathrm{e}}/\nu$ is the Reynolds number.

3 Chebyshev polynomials and properties

The Chebyshev polynomials and their properties are discussed in this section briefly. The Chebyshev polynomials T_m of the mth-order must satisfy

$$(1-\eta^2)\frac{\mathrm{d}^2T_m(\eta)}{\mathrm{d}\eta^2} - \eta\frac{\mathrm{d}T_m(\eta)}{\mathrm{d}\eta} + m^2T_m(\eta) = 0.$$

The Chebyshev polynomials can be attained via the recurrence relation stated as follows:

$$\begin{cases} T_0(\eta) = 1, \quad T_1(\eta) = \eta, \\ T_{m+1}(\eta) = 2\eta T_m(\eta) - T_{m-1}(\eta), \quad m \geqslant 1. \end{cases}$$

The Chebyshev polynomials of the third kind are given as follows[8,30–32]:

$$C_m(\eta) = \cos\Big(\Big(m+\frac{1}{2}\Big)\theta\Big)\cos\frac{\theta}{2},$$

where $\cos\theta = \eta$. The Chebyshev polynomials of the third kind are orthogonal in $[-1,1]$ w.r.t. the weight function $w = \sqrt{\frac{1+\eta}{1-\eta}}$, i.e.,

$$\int_{-1}^{1} C_m(\eta)C_n(\eta)w\mathrm{d}\eta = \begin{cases} 0, & m \neq n, \\ \pi, & m = n. \end{cases}$$

The third kind of Cheyshev polyomials can be obtained by means of the following relation[8,30–32]:

$$\begin{cases} V_0(\eta) = 1, \quad V_1(\eta) = 2\eta - 1, \\ V_m(\eta) = 2\eta V_{m-1}(\eta) - V_{m-2}(\eta), \quad m \geqslant 2. \end{cases} \tag{12}$$

The properties of the third kind Chebyshev polynomials are as follows[8,30–32]:

(i) $C_m(1) = 1, \quad C_m(-1) = (-1)^m(2m+1).$

(ii) $$\frac{\mathrm{d}^nC_m(\eta)}{\mathrm{d}x^n} = \frac{\sqrt{\pi}(m+n)}{2^n(m-n)} \begin{cases} \dfrac{1}{\Gamma\big(n+\frac{1}{2}\big)}, & x = 1, \\ \dfrac{(-1)^{m+n}(2m+1)}{2\Gamma\big(n+\frac{1}{2}\big)}, & x = -1. \end{cases}$$

3.1 Wavelets and Chebyshev wavelets

Many numerical algorithms have been proposed to study non-Newton fluids. The wavelet method is one of the most widely used one among all these methods. It has been successfully used in the engineering field, the physical field, and biological sciences[8,30–32]. The Chebyshev wavelets of the third kind are defined as follows[30]:

$$\psi_{p,q}(\eta)=\begin{cases}2^{\frac{k}{2}}\widetilde{C}_q(2^k\eta-(2p-1)), & \dfrac{p-1}{2^{k-1}}\leqslant\eta\leqslant\dfrac{p}{2^{k-1}},\\ 0, \quad \text{otherwise}, \end{cases} \tag{13}$$

where

$$\widetilde{C}_q=\frac{1}{\sqrt{\pi}}C_q, \quad q=0,1,2,\cdots,M-1, \quad p=0,1,\cdots,2^{k-1}.$$

$C_q(\eta)$ is the qth-order Chebyshev polynomials of the third kind. A function $g(\eta)$ from the $L^2(\mathbb{R})$-space defined in $[0,1)$ can be expanded in terms of the third kind Chebyshev wavelets as follows:

$$g(\eta)=\sum_{p=1}^{\infty}\sum_{q=0}^{\infty}\xi_{p,q}\psi_{p,q}(\eta), \tag{14}$$

where

$$\xi_{p,q}=\int_0^1 g(\eta)\psi_{p,q}(\eta)w_p\mathrm{d}\eta.$$

Equation (14) can be truncated as follows:

$$g(\eta)=\sum_{p=1}^{2^{k-1}}\sum_{q=0}^{M-1}\xi_{p,q}\psi_{p,q}(\eta)=\mathcal{M}^{\mathrm{T}}\boldsymbol{\psi}(\eta), \tag{15}$$

where $\mathcal{M}$ and $\boldsymbol{\psi}(\eta)$ are $2^{k-1}M\times 1$ orders, which are given in Refs. [8] and [30]–[32].

3.2 Modified Chebyshev wavelet method (MCWM) and solution procedure

This section is devoted to a comprehensive study of the MCWM[8] and its applications to solve the flow problem (7)–(10). The solution procedure for the MCWM is explained as follows:

Step 1 Consider the problem

$$\begin{aligned}&(1+\wedge F''(\eta))F'''(\eta)-F'^2(\eta)+\Big(F(\eta)-\frac{A}{2}\eta\Big)F''(\eta)-(M+A)(F'(\eta)-r)\\&\pm\lambda(\theta(\eta)+R\phi(\eta))+r^2=0,\end{aligned} \tag{16}$$

$$(1+Rd)\theta''(\eta)+Pr\Big(F(\eta)-\frac{A}{2}\eta\Big)\theta'(\eta)+PrDu\phi''(\eta)=0, \tag{17}$$

$$\phi''(\eta)+Sc\Big(F(\eta)-\frac{A}{2}\eta\Big)\phi'(\eta)+SrSc\theta''(\eta)=0. \tag{18}$$

Step 2 Introduce the following trial solutions suggested by the traditional Chebyshev

wavelet method to solve Eqs. (16)–(18):

$$\widetilde{F} = \sum_{p=1}^{2^{k-1}} \sum_{q=0}^{M-1} \xi_{p,q}^{1} \psi_{p,q}(\eta) = \mathcal{M}_1^{\mathrm{T}} \boldsymbol{\psi}(\eta), \tag{19}$$

$$\widetilde{\theta} = \sum_{p=1}^{2^{k-1}} \sum_{q=0}^{M-1} \xi_{p,q}^{2} \psi_{p,q}(\eta) = \mathcal{M}_2^{\mathrm{T}} \boldsymbol{\psi}(\eta), \tag{20}$$

$$\widetilde{\phi} = \sum_{p=1}^{2^{k-1}} \sum_{q=0}^{M-1} \xi_{p,q}^{3} \psi_{p,q}(\eta) = \mathcal{M}_3^{\mathrm{T}} \boldsymbol{\psi}(\eta), \tag{21}$$

where $\mathcal{M}_i$ $(i = 1, 2, 3)$ and $\boldsymbol{\psi}(\eta)$ are presented in Ref. [8]. The trial solutions (19)–(21) can be rewritten as follows:

$$\widetilde{F} = \boldsymbol{\gamma}_1 \boldsymbol{\chi}(\eta), \quad \widetilde{\theta} = \boldsymbol{\gamma}_2 \boldsymbol{\chi}(\eta), \quad \widetilde{\phi} = \boldsymbol{\gamma}_1 \boldsymbol{\chi}(\eta), \tag{22}$$

where $\boldsymbol{\chi}(\eta)$ and $\boldsymbol{\gamma}_i$ $(i = 1, 2, 3)$ are presented in Ref. [8]. Now, we introduce a new set of unknowns $\{\zeta_0^i, \zeta_1^i, \zeta_2^i, \cdots\}$ for $i = 1, 2, 3$ such that

$$\begin{cases} \xi_{0,1}^i - \sqrt{3}\xi_{1,1}^i + \sqrt{5}\xi_{1,2}^i - \cdots = \zeta_0^i, \\ 2\sqrt{3}\xi_{1,1}^i - 6\sqrt{5}\xi_{1,2}^i + 12\sqrt{7}\xi_{1,3}^i + \cdots = \zeta_1^i, \end{cases} \tag{23}$$

$$\begin{cases} 6\sqrt{5}\xi_{1,2}^i - 30\sqrt{7}\xi_{1,3}^i + \cdots = \zeta_2^i, \\ 20\sqrt{7}\xi_{1,3}^i + \cdots = \zeta_3^i, \\ \quad \vdots \end{cases} \tag{24}$$

The trial solutions given in Ref. [8] takes the following forms after incorporating Eqs. (23) and (24):

$$\widetilde{F}(\eta) = \sum_{n=0}^{M} \zeta_n^1 \eta^n, \quad \widetilde{\theta}(\eta) = \sum_{n=0}^{M} \zeta_n^2 \eta^n, \quad \widetilde{\phi}(\eta) = \sum_{n=0}^{M} \zeta_n^3 \eta^n. \tag{25}$$

After incorporating the boundary conditions in Eq. (10), we can rewrite the trial solutions in Eq. (25) as follows:

$$\widetilde{F}(\eta) = S + \eta - \frac{1}{2\eta_\infty}(1 - r)\eta^2 + \sum_{k=1}^{M-3} \zeta_k^1 \Big(\eta^k - \frac{k+2}{2}\eta_\infty^k\Big)\eta^2, \tag{26}$$

$$\widetilde{\theta}(\eta) = 1 - \frac{1}{\eta_\infty}\eta + \sum_{k=1}^{M-2} \zeta_k^2 (\eta^k - \eta_\infty^k)\eta, \tag{27}$$

$$\widetilde{\phi}(\eta) = 1 - \frac{1}{\eta_\infty}\eta + \sum_{k=1}^{M-2} \zeta_k^3 (\eta^k - \eta_\infty^k)\eta. \tag{28}$$

Step 3 The residuals for $F(\eta)$, $\theta(\eta)$, and $\phi(\eta)$ can be obtained after inserting the trial

solutions (26)–(28) into Eqs. (16)–(18) as follows:

$$R_F = (1+\Lambda\widetilde{F}^{''}(\eta))\widetilde{F}^{'''}(\eta) - \widetilde{F}^{'^2}(\eta) + \Big(\widetilde{F}(\eta) - \frac{A}{2}\eta\Big)\widetilde{F}^{''}(\eta) - (M+A)(\widetilde{F}^{'}(\eta) - r) \pm \lambda(\widetilde{\theta}(\eta) + R\widetilde{\phi}(\eta)) + r^2, \tag{29}$$

$$R_\theta = (1+Rd)\widetilde{\theta}^{''}(\eta) + Pr\Big(\widetilde{F}(\eta) - \frac{A}{2}\eta\Big)\widetilde{\theta}^{'}(\eta) + PrDu\widetilde{\phi}^{''}(\eta), \tag{30}$$

$$R_\phi = \widetilde{\phi}^{''}(\eta) + Sc\Big(\widetilde{F}(\eta) - \frac{A}{2}\eta\Big)\widetilde{\phi}^{'}(\eta) + SrSc\widetilde{\theta}^{''}(\eta). \tag{31}$$

Step 4 In Step 3, the given problem is reduced to an equivalent number of algebraic equations having $3M-7$ unknowns. Therefore, to find the unknowns $\zeta_0^i, \zeta_1^i, \zeta_2^i, \cdots$ $(i=1,2,3)$, we need $3M-7$ equations. Here, we use the collocation points for Eqs. (29)–(31) to generate the equations as $\eta_n = \frac{n}{M}\eta_\infty$ $(n=1,2,\cdots,M-3)$, $\eta_n = \frac{n}{M}\eta_\infty$ $(n=1,2,\cdots,M-2)$, and $\eta_n = \frac{n}{M}\eta_\infty$ $(n=1,2,\cdots,M-2)$, respectively.

Step 5 After solving the system of equations achieved in the last step, we can obtain the values of the unknowns ζ's. The values of ξ's can be obtained by using the relations (23) and (24). Finally, we can obtain the approximate solutions of the problem (7)–(10) after substituting the values of ξ's into Eqs. (19)–(21).

4 Results and discussion

Herein, the thermal radiation effects and the buoyancy assisting and opposing effects on the stagnation point flow of the Williamson nanofluid are briefly discussed. The flow is 2D unsteady, viscous, and incompressible over a porous stretching surface. The combined effects of the thermal radiation and the conduction or convection in the presence of buoyancy forces appear in various areas of science including spacecrafts, high temperature heat exchangers, combustion chambers, thermal insulations, industrial furnaces, etc. In account of these practical applications, a model study is conducted. A wavelet algorithm is adopted to analyze the problem theoretically. The emerging parameters, the physical quantities, and their effects on the velocity $\widetilde{F}^{'}(\eta)$, the temperature $\theta(\eta)$, and the concentration $\phi(\eta)$ of the fluid are plotted graphically and described on the basis of the already reported values of parameters[10,23,33–35]. Various suitable ranges for the dimensionless velocity, the temperature, and the concentration are deliberated, and particular exertions are made on the effects of these parameters on the fluid flow and heat transport. The selection of the values for the aforementioned parameters is based on the physical characteristics of the proposed model, and is related to the stability of the solution. A tabular form of comparison with the existing literature is enclosed in the discussion part. Table 1 shows the credibility of our technique. The comparison analysis with the existing literature[10,33–35] is endorsing that wavelet algorithms are efficient and compatible tools to tackle nonlinear flow problems.

Table 1 Comparison of the present results for $Re_x^{-1/2}Nu$ with the existing results in Refs. [10] and [33]–[35] for different values of Pr when $r = M = \Lambda = A = S = \lambda = 0$

η	Ref. [33]	Ref. [34]	Ref. [35]	Ref. [10]	MCWM
0.01	0.029 44	0.029 4	0.029 42	0.029 425	0.029 425 210 4
0.72	1.088 55	1.088 5	1.088 53	1.088 575	1.088 575 452 1
1.00	1.333 34	1.333 3	1.333 34	1.333 270	1.333 270 145 2
3.00	2.509 71	2.509 7	2.509 72	2.509 465	2.509 465 120 4

4.1 Behavior of the velocity profiles

The effects of various emerging parameters, including the Hartmann number M, the ratio parameter λ, the stagnation parameter r, the unsteadiness parameter A, the Williamson fluid parameter Λ, and the Suction parameter S, on the velocity profiles $F'(\eta)$ are shown in Figs. 2–7 according to Eqs. (2)–(7).

Figure 2 is plotted to show the behavior of a magnetic parameter for the assisting and opposing flow regions. It is noted that, when M increases, $F'(\eta)$ is enhanced for the opposing case while decreases for the assisting case. Figure 3 shows the effects of the ratio parameter λ. It can be clearly seen that, when λ increases the velocity increases for the assisting case while decreases for the opposing case. The variation is significant for higher values of the ratio parameter for both the assisting and opposing cases.

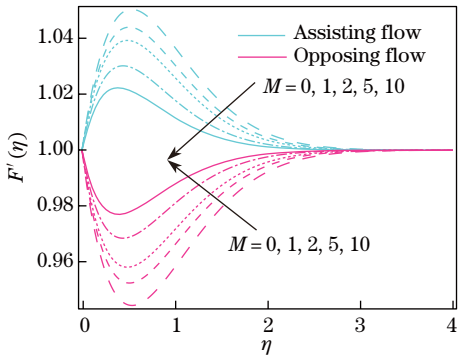

Fig. 2 Variations in M and effects on $F'(\eta)$, where $r = 1$, and $A = l = \Lambda = R = 0.5$ (color online)

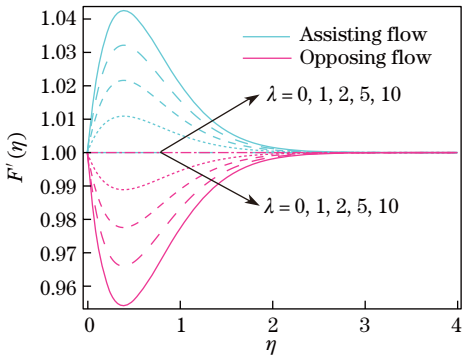

Fig. 3 Variations in λ and effects on $F'(\eta)$, where $r = 1$, $\Lambda = 0.5$, $R = 0.25$, and $M = A = 0.5$ (color online)

The variations in the stagnation point parameter r are presented in Fig. 4. It can be seen that an increase in the values of r results in an increase in the velocity profile $F'(\eta)$ for both the assisting and opposing cases. It is perceived that the assisting effects are more significant than the opposing ones. As shown in Fig. 5, when the unsteadiness parameter A increases, the velocity of the fluid increases for the assisting case while decreases for the opposing case.

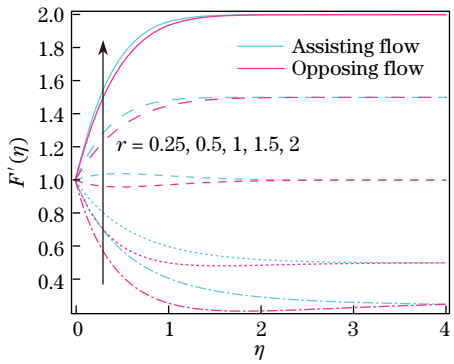

Fig. 4 Variations in r and effects on $F'(\eta)$, where $M = 2$, $= 0.2$, and $R = l = A = 0.5$ (color online)

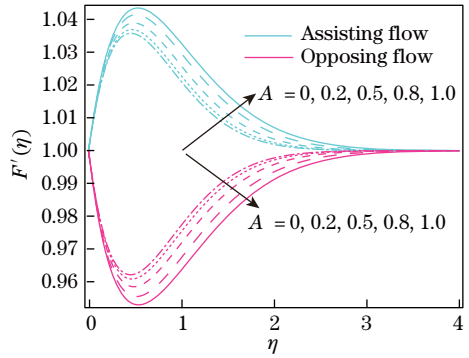

Fig. 5 Variations in A and effects on $F'(\eta)$, where $M = 2$, $\Lambda = R = l = 0.5$, and $r = 0.5$ (color online)

Figure 6 shows the effects of the Williamson parameter Λ on the velocity profiles. From the figure, we can see that when Λ increases, the velocity decreases for both the assisting and opposing cases. Moreover, Williamson parameter Λ has negligible effects on the velocity profile.

Figure 7 shows the effects of the suction parameter S on the velocity profiles. It can be seen that, when S increases, the velocity decreases for the opposing case while increases for the assisting case.

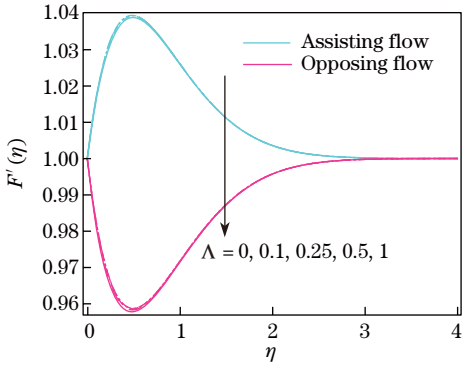

Fig. 6 Effects of Λ on $F'(\eta)$, where $M = 2$, $A = l = R = 0.5$, and $r = 1$ (color online)

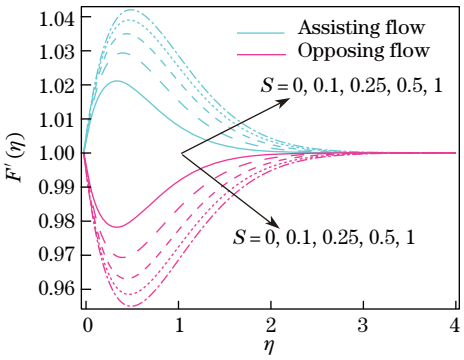

Fig. 7 Effects of S on $F'(\eta)$, where $M = 2$, $A = l = \Lambda = R = 0.5$, and $r = 1$ (color online)

4.2 Behaviors of the temperature profiles

The buoyancy (assisting and opposing) effects with various physical parameters on the temperature profiles are shown in Figs. 8–11.

Figure 8 shows the effects of the unsteadiness parameter A on the temperature profiles. It can be seen that, when A increases, the temperature increases for both the assisting and opposing cases, while the effects of the opposing flow are a little more dominant than those of the assisting flow.

Figure 9 shows the effects of the radiation parameter Rd on the temperature profiles. It can be seen that, when Rd increases, the temperature increases for both the assisting and opposing cases, while the opposing effects are more significant than the assisting ones.

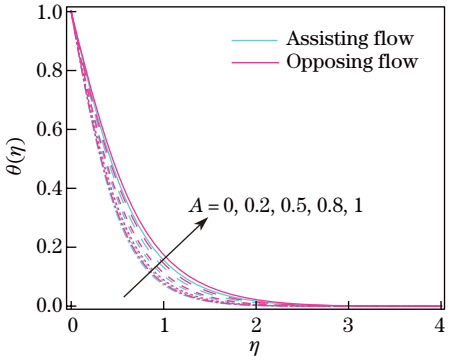

Fig. 8 Effects of A on $\theta(\eta)$, where $Sr = Rd = Du = 0.5$, $Sc = 2$, and $Pr = 6.2$ (color online)

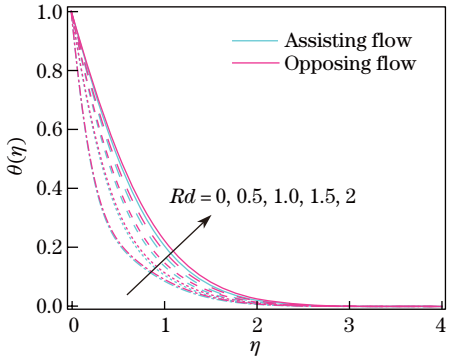

Fig. 9 Effects of Rd on $\theta(\eta)$, where $Sr = A = Du = 0.5$, $Sc = 2$, and $Pr = 6.2$ (color online)

Figure 10 shows the effects of the Dufour parameter Du on the temperature profiles. It can be seen that, when Du increases, the temperature increases for both the assisting and opposing cases, while the opposing effects are more prevailing than those of the assisting ones.

Figure 11 shows the effects of the Prandtl number Pr on the temperature profiles. It can be seen that, when Pr increases, the temperature decreases for both the assisting and opposing cases, while the assisting effects are more significant than those of the opposing ones.

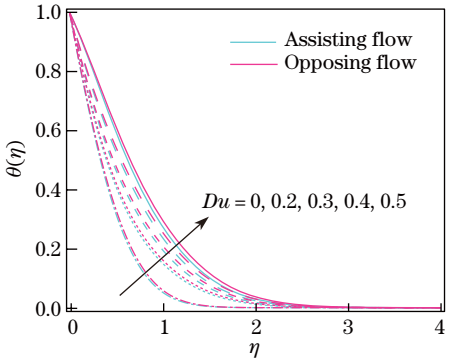

Fig. 10 Effects of Du on $\theta(\eta)$, where $Sr = 0.2$, $A = Rd = 0.5$, $Sc = 2$, $Pr = 6.2$ (color online)

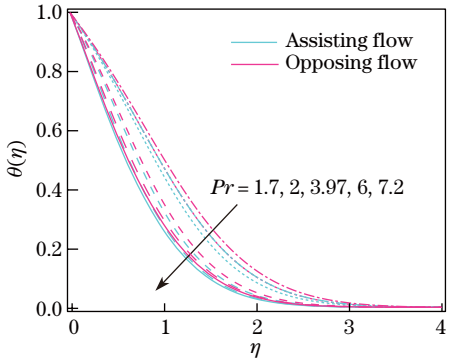

Fig. 11 Effects of Pr on $\theta(\eta)$, where $Sr = 0.2$, $A = Rd = 0.5$, $Sc = 2$, and $Du = 0.5$ (color online)

4.3 Behaviors of the concentration profiles

Figures 12 and 13 are plotted to describe the behaviors of the concentration profiles $\phi(\eta)$. From these figures, we can see that, when the Soret number Sr increases, the concentration $\phi(\eta)$ increases for both the assisting and opposing cases, and the opposing effects are a slightly dominant as compared with the assisting ones (see Fig. 12). However, when the Schmidt number Sc increases, the concentration $\phi(\eta)$ decreases for both the assisting and opposing cases, and the assisting effects are more significant than the opposing ones.

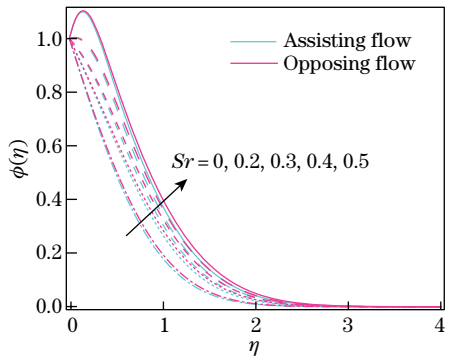

Fig. 12 Effects of Sr on $\phi(\eta)$, where $Du = 0.2$, $A = Rd = 0.5$, $Sc = 24$, and $Pr = 6.2$ (color online)

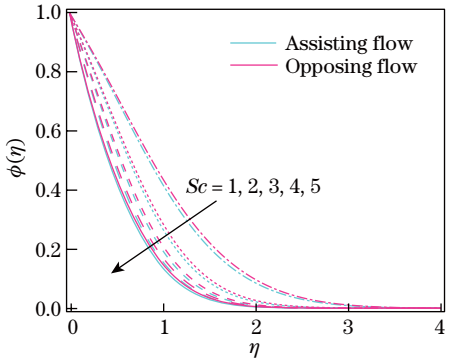

Fig. 13 Effects of Sc on $\phi(\eta)$, where $Du = 0.2$, $A = Rd = 0.5$, $Sr = 24$, and $Pr = 6.2$ (color online)

4.4 Behaviors of the physical quantities

Figures 14–18 show the effects of buoyancy and the emerging parameters on the physical quantities briefly.

Figure 14 shows the effects of Λ, M, and S on the skin friction coefficient. The behaviors of the skin friction coefficient for the buoyancy effects and various values of the unsteadiness parameter A, the stagnation parameter r, and the ration parameter Λ are also presented. From Fig. 14, we can see that, when A or S increases, the skin friction increases for the assisting case while decreases for the opposing case. Moreover, The effects of λ provide higher values of the skin friction coefficient for the assisting case while lower values for the opposing case. When the magnetic parameter M increases, the skin friction coefficient increases for both the assisting and opposing cases, while the assisting effects are more significant than the opposing ones.

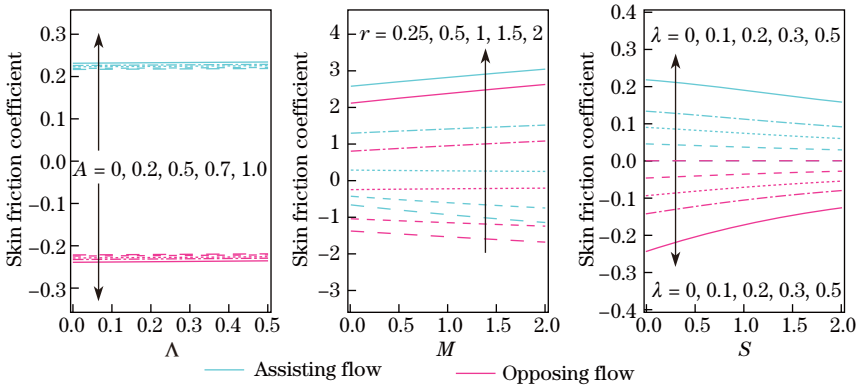

Fig. 14 Effects of Λ, M, and S on the skin friction coefficient (color online)

Figure 15 is designed to show the effects of the Dufour number Du for the assisting and opposing cases. It can be seen that, when Du increases, the local Nusselt number Nu decreases for both the assisting and opposing cases. Here, it is important to mention that the opposing case provides a more significant decrease than the assisting case.

Figure 16 shows the effects of the Prandtl number Pr for the assisting and opposing cases. It can be seen that, when Pr increases, the local Nusselt number Nu increases for both the assisting and opposing cases, and the assisting effects are more dominant than the opposing ones.

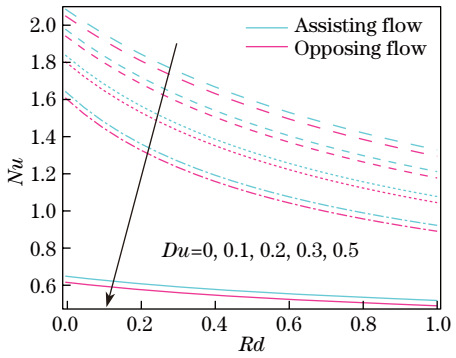

Fig. 15 Effects of Du on the Nusselt number (color online)

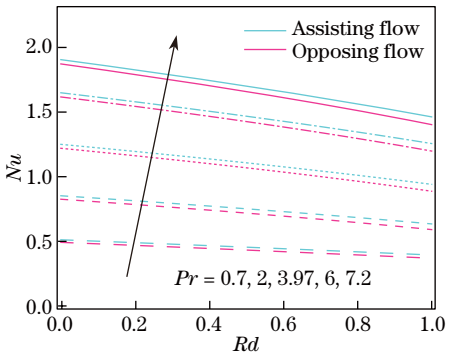

Fig. 16 Effects of Pr on the Nusselt number (color online)

Figures 17 and 18 show the effects of the Soret number Sr and the Prandtl number Pr for the assisting and opposing cases. It can be seen that, when Sr or Pr increases, the Sherwood number decreases, and the opposing effects are more dominant than the assisting ones.

5 Concluding remarks

A wavelet analysis is presented for the effects of buoyancy forces on the stagnation point flow of the Williamson nanofluid with thermal radiation. The set of flow equations are reduced to a nonlinear ordinary differential equation system with the appropriate similarity method, and are numerically tackled via a new wavelet algorithm based on Chebyshev polynomials. The key findings are as follows:

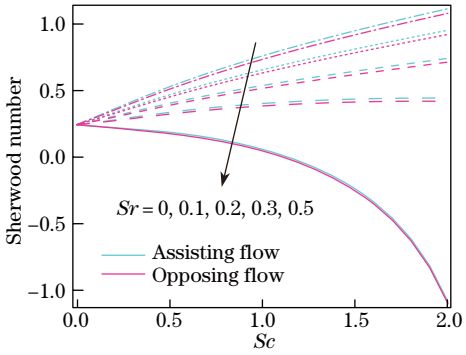

Fig. 17 Effects of Sr on the Sherwood number (color online)

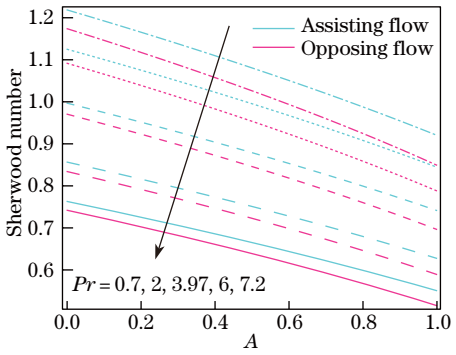

Fig. 18 Effects of Pr on the Sherwood number (color online)

(i) When A, S, or λ increases, $F'(\eta)$ increases for the assisting case while decreases for the opposing case. When the magnetic parameter increases, the velocity increases for the opposing case while decreases for the assisting case.

(ii) When Du, Rd, or A increases, the temperature increases for both the assisting and opposing cases. When Pr increases, the temperature decreases. Moreover, the opposing effects are slightly more dominant than the assisting ones.

(iii) The concentration decreases when Sr increases while increases when Sc increases. It is perceived that the assisting force causes more decrease than the opposing one.

(iv) When r increases, the skin friction coefficient increases for both the assisting and opposing cases. When λ or A increases, the skin friction coefficient increases in the assisting region while decreases in the opposing region.

(v) When Pr increases, the local Nusselt number increases while the Sherwood number decreases. When Sr or Sc increases, the Sherwood and Nusselt numbers decrease.

(vi) A worthy comparison of outcomes obtained via the MCWM is presented. It is evident that the MCWM is very accurate, and could be extended to other complex natural nonlinear flow problems.

Acknowledgements The authors are grateful to the reviewers and editor for suggesting suitable changes in the original manuscript. The first author is also grateful to the China Scholarship Council (CSC) for the financial assistance.

References

[1] HIEMENZ, K. Die grenzschicht an einem in den gleichförmigen Flüssigkeitsstrom eingetauchten geraden Kreiszylinder. *Dingler's Polytechnic Journal*, **326**, 321–324 (1911)

[2] HOMANN, F. and ANGEW, Z. Der einfluss grosser Zähigkeit bei der Strömung um den zylinder und um die Kugel. *Journal of Applied Mathematics and Mechanics*, **16**, 153–164 (1936)

[3] MAKINDE, O. D., KHAN, W. A., and KHAN, Z. H. Buoyancy effects on MHD stagnation point flow and heat transfer of a nanofluid past a convectively heated stretching/shrinking sheet. *International Journal of Heat and Mass Transfer*, **62**, 526–533 (2013)

[4] HAQ, R. U., NADEEM, S., KHAN, Z. H., and AKBAR, N. S. Thermal radiation and slip effects on MHD stagnation point flow of nanofluid over a stretching sheet. *Physica E*: *Low-Dimensional Systems and Nanostructures*, **65**, 17–23 (2015)

[5] HAYAT, T., KHAN, M. I., WAQAS, M., ALSAEDI, A., and FAROOQ, M. Numerical simulation for melting heat transfer and radiation effects in stagnation point flow of carbon-water nanofluid. *Computer Methods in Applied Mechanics and Engineering*, **315**, 1011–1024 (2017)

[6] TARAKARAMU, N. and NARAYANA, P. V. Nonlinear thermal radiation and Joule heating effects on MHD stagnation point flow of a nanofluid over a convectively heated stretching surface. *Journal of Nanofluids*, **8**, 1066–1075 (2019)

[7] PAL, D. Heat and mass transfer in stagnation-point flow towards a stretching surface in the presence of buoyancy force and thermal radiation. *Meccanica*, **44**, 145–158 (2009)

[8] USMAN, M., ZUBAIR, T., HAMID, M., HAQ, R. U., and WANG, W. Wavelets solution of MHD 3-D fluid flow in the presence of slip and thermal radiation effects. *Physics of Fluids*, **30**, 023104 (2018)

[9] MOHYUD-DIN, S. T., USMAN, M., AFAQ, K., HAMID, M., and WANG, W. Examination of carbon-water nanofluid flow with thermal radiation under the effect of Marangoni convection. *Engineering Computations*, **34**, 2330–2343 (2017)

[10] HAYAT, T., QASIM, M., SHEHZAD, S. A., and ALSAEDI, A. Unsteady stagnation point flow of second grade fluid with variable free stream. *Alexandria Engineering Journal*, **53**, 455–461 (2014)

[11] BOULAHIA, Z., WAKIF, A., and SEHAQUI, R. Heat transfer and cu-water nanofluid flow in a ventilated cavity having central cooling cylinder and heated from the below considering three different outlet port locations. *Frontiers in Heat and Mass Transfer*, **11**, 11 (2018)

[12] SAIDUR, R., LEONG, K. Y., and MOHAMMAD, H. A review on applications and challenges of nanofluids. *Renewable and Sustainable Energy Reviews*, **15**, 1646–1668 (2011)

[13] CHOI, S. U. S. Enhancing thermal conductivity of fluids with nanoparticle. *Developments and Applications of Non-Newtonian Flows*, Springer, New York (1995)

[14] BUONGIORNO, J. Convective transport in nanofluids. *Journal of Heat Transfer*, **128**, 240–250 (2006)

[15] TIWARI, R. K. and DAS, M. K. Heat transfer augmentation in a two-sided lid-driven differentially heated square cavity utilizing nanofluids. *International Journal of Heat and Mass Transfer*, **50**, 2002–2018 (2007)

[16] HAYAT, T., ABBASI, F. M., AL-YAMI, M., and MONAQUEL, S. Slip and Joule heating effects in mixed convection peristaltic transport of nanofluid with Soret and Dufour effects. *Journal of Molecular Liquids*, **194**, 93–99 (2014)

[17] REDDY, P. S. and CHAMKHA, A. J. Soret and Dufour effects on MHD convective flow of Al_2O_3-water and TiO_2-water nanofluids past a stretching sheet in porous media with heat generation/absorption. *Advanced Powder Technology*, **27**, 1207–1218 (2016)

[18] HAYAT, T., FAROOQ, S., ALSAEDI, A., and AHMAD, B. Numerical study for Soret and Dufour effects on mixed convective peristalsis of Oldroyd 8-constants fluid. *International Journal of Thermal Sciences*, **112**, 68–81 (2017)

[19] HAMID, M., USMAN, M., ZUBAIR, T., HAQ, R. U., and WANG, W. Shape effects of MoS_2 nanoparticles on rotating flow of nanofluid along a stretching surface with variable thermal conductivity: a Galerkin approach. *International Journal of Heat and Mass Transfer*, **124**, 706–714 (2018)

[20] USMAN, M., HAMID, M., MOHYUD-DIN, S. T., WAHEED, A., and WANG, W. Exploration of uniform heat flux on the flow and heat transportation of ferrofluids along a smooth plate: comparative investigation. *International Journal of Biomathematics*, **11**, 1850048 (2018)

[21] SHEIKHOLESLAMI, M. and ROKNI, H. B. Numerical simulation for impact of Coulomb force on nanofluid heat transfer in a porous enclosure in presence of thermal radiation. *International Journal of Heat and Mass Transfer*, **118**, 823–831 (2018)

[22] WILLIAMSON, R. V. The flow of pseudoplastic materials. *Industrial and Engineering Chemistry*, **21**, 1108–1111 (1929)

[23] AMANULLA, C. H., NAGENDRA, N., RAO, A. S., BEG, O. A., and KADIR, A. Numerical exploration of thermal radiation and Biot number effects on the flow of a non-Newtonian MHD Williamson fluid over a vertical convective surface. *Heat Transfer-Asian Research*, **47**, 286–304 (2018)

[24] JAIN, S. and PARMAR, A. Radiation effect on MHD Williamson fluid flow over stretching cylinder through porous medium with heat source. *Applications of Fluid Dynamics*, Springer, Singapore (2018)

[25] HAMID, M., USMAN, M., KHAN, Z. H., HAQ, R. U., and WANG, W. Numerical study of unsteady MHD flow of Williamson nanofluid in a permeable channel with heat source/sink and thermal radiation. *The European Physical Journal Plus*, **133**, 527 (2018)

[26] MUSTAFA, M., KHAN, J. A., HAYAT, T., and ALSAEDI, A. Buoyancy effects on the MHD nanofluid flow past a vertical surface with chemical reaction and activation energy. *International Journal of Heat and Mass Transfer*, **108**, 1340–1346 (2017)

[27] NOOR, N. F., HAQ, R. U., NADEEM, S., and HASHIM, I. Mixed convection stagnation flow of a micropolar nanofluid along a vertically stretching surface with slip effects. *Meccanica*, **50**, 2007–2022 (2015)

[28] HAQ, R. U., NADEEM, S., AKBAR, N. S., and KHAN, Z. H. Buoyancy and radiation effect on stagnation point flow of micropolar nanofluid along a vertically convective stretching surface. *IEEE Transactions on Nanotechnology*, **14**, 42–50 (2015)

[29] AKBAR, N. S., TRIPATHI, D., KHAN, Z. H., and BEG, O. A. A numerical study of magnetohydrodynamic transport of nanofluids over a vertical stretching sheet with exponential temperature-dependent viscosity and buoyancy effects. *Chemical Physics Letters*, **661**, 20–30 (2016)

[30] DOHA, E. H., ABD-ELHAMEED, W. M., and ALSUYUTI, M. M. On using third and fourth kinds Chebyshev polynomials for solving the integrated forms of high odd-order linear boundary value problems. *Journal of the Egyptian Mathematical Society*, **23**, 397–405 (2015)

[31] ZHOU, F. and XU, X. The third kind Chebyshev wavelets collocation method for solving the time-fractional convection diffusion equations with variable coefficients. *Applied Mathematics and Computation*, **280**, 11–29 (2016)

[32] ABD-ELHAMEED, W. M., DOHA, E. H., and YOUSSRI, Y. H. New wavelets collocation method for solving second-order multipoint boundary value problems using Chebyshev polynomials of third and fourth kinds. *Abstract and Applied Analysis*, **2013**, 542839 (2013)

[33] MUKHOPADHYAY, S. Effect of thermal radiation on unsteady mixed convection flow and heat transfer over a porous stretching surface in a porous medium. *International Journal of Heat and Mass Transfer*, **52**, 3261–3265 (2009)

[34] GRUBKA, L. J. and BOBBA, K. M. Heat transfer characteristics of a continuous stretching surface with variable temperature. *Journal of Heat Transfer*, **107**, 248–250 (1985)

[35] CHEN, C. H. Laminar mixed convection adjacent to vertical, continuously stretching sheets. *Heat and Mass Transfer*, **33**, 471–476 (1998)